Michigan Technological University

Digital Commons @ Michigan Tech

2003

Quantitative shape measurements of distal volcanic ash

William I. Rose
Michigan Technological University

Colleen M. Riley
Michigan Technological University

Gregg J. Bluth
Michigan Technological University

Follow this and additional works at: https://digitalcommons.mtu.edu/geo-fp

Part of the Geology Commons, Mining Engineering Commons, and the Other Engineering Commons

Follow this and additional works at: https://digitalcommons.mtu.edu/geo-fp

Part of the Geology Commons, Mining Engineering Commons, and the Other Engineering Commons

Quantitative shape measurements of distal volcanic ash

Colleen M. Riley,[1] William I. Rose, and Gregg J. S. Bluth

Department of Geological Engineering and Sciences, Michigan Technological University, Houghton, Michigan, USA

[1] Large-scale volcanic eruptions produce fine ash (<200 μm) which has a long atmospheric residence time (1 hour or more) and can be transported great distances from the volcanic source, thus, becoming a hazard to aircraft and public health. Ash particles have irregular shapes, so data on particle shape, size, and terminal velocities are needed to understand how the irregular-shaped particles affect transport processes and radiative transfer measurements. In this study, a methodology was developed to characterize particle shapes, sizes, and terminal velocities for three ash samples of different compositions. The shape and size of 2500 particles from (1) distal fallout (∼100 km) of the 14 October 1974 Fuego eruption (basaltic), (2) the secondary maxima (∼250 km) of the 18 August 1992 Spurr eruption (andesitic), and (3) the Miocene Ash Hollow member, Nebraska (rhyolitic) were measured using image analysis techniques. Samples were sorted into 10 to 19 terminal velocity groups (0.6–59.0 cm/s) using an air elutriation device. Grain-size distributions for the samples were measured using laser diffraction. Aspect ratio, feret diameter, and perimeter measurements were found to be the most useful descriptors of how particle shape affects terminal velocity. These measurement values show particle shape differs greatly from a sphere (commonly used in models and algorithms). The diameters of ash particles were 10–120% larger than ideal spheres at the same terminal velocity, indicating that irregular particle shape greatly increases drag. Gas-adsorption derived surface areas are 1 to 2 orders of magnitude higher than calculated surface areas based on measured dimensions and simple geometry, indicating that particle shapes are highly irregular. Correction factors for surface area were derived from the ash sample measurements so that surface areas calculated by assuming spherical particle shapes can be corrected to reflect more realistic values. *INDEX TERMS:* 0305 Atmospheric Composition and Structure: Aerosols and particles (0345, 4801); 3640 Mineralogy and Petrology: Igneous petrology; 8404 Volcanology: Ash deposits; 8414 Volcanology: Eruption mechanisms; 8494 Volcanology: Instruments and techniques; *KEYWORDS:* volcanic ash, Spurr, Fuego, Ogallala, grain size, terminal velocity

1. Introduction

[2] Large-scale volcanic eruptions that inject ash particles into the stratosphere are a significant hazard to populations both near and far from the volcano as well as aircraft flying through the eruption cloud [*Casadevall and Krohn*, 1995; *Sparks et al.*, 1997]. The coarser (>1 mm in diameter) pyroclastic material that is injected into the atmosphere by such an eruption falls out within an hour but remaining finer particles (<10 μm) can stay suspended for days to months [*Rose et al.*, 2001]. These finer particles can be transported great distances and deposit irregularly and in unusually thick amounts far from the volcanic source [*Sarna-Wojcicki et al.*, 1981; *Swinehart et al.*, 1985; *Glaze and Self*, 1991;

Hildreth and Drake, 1992; *Ernst et al.*, 1996]. The distance traveled by ash particles is dependent on several factors including particle shape which affects the aerodynamic properties responsible for particle separation and fallout (see, e.g., *Bursik et al.* [1998] for a brief review). Aggregation of particles is also affected because particle surface area, electrostatic charge, and the possibility of mechanical interlocking are related to shape [*Gilbert and Lane*, 1994]. The ability of satellite sensors to accurately quantify ash particle concentrations and effective radius relies on accurate shape characteristics because particle shape may strongly influence electromagnetic scattering [*Wen and Rose*, 1994; *Krotkov et al.*, 1999b].

[3] Despite their irregular shape, ash particles are most commonly modeled as spheres in both transport modeling experiments [*Brazier et al.*, 1982; *Carey and Sigurdsson*, 1982; *Suzuki*, 1983; *Armienti et al.*, 1988; *Glaze and Self*, 1991; *Sparks et al.*, 1992; *Jarzemba et al.*, 1997] and remote sensing algorithms [*Wen and Rose*, 1994; *Krotkov et al.*, 1997] primarily because no quantitative description of

---

[1]Now at School of Education and Social Policy, Northwestern University, Evanston, Illinois, USA.
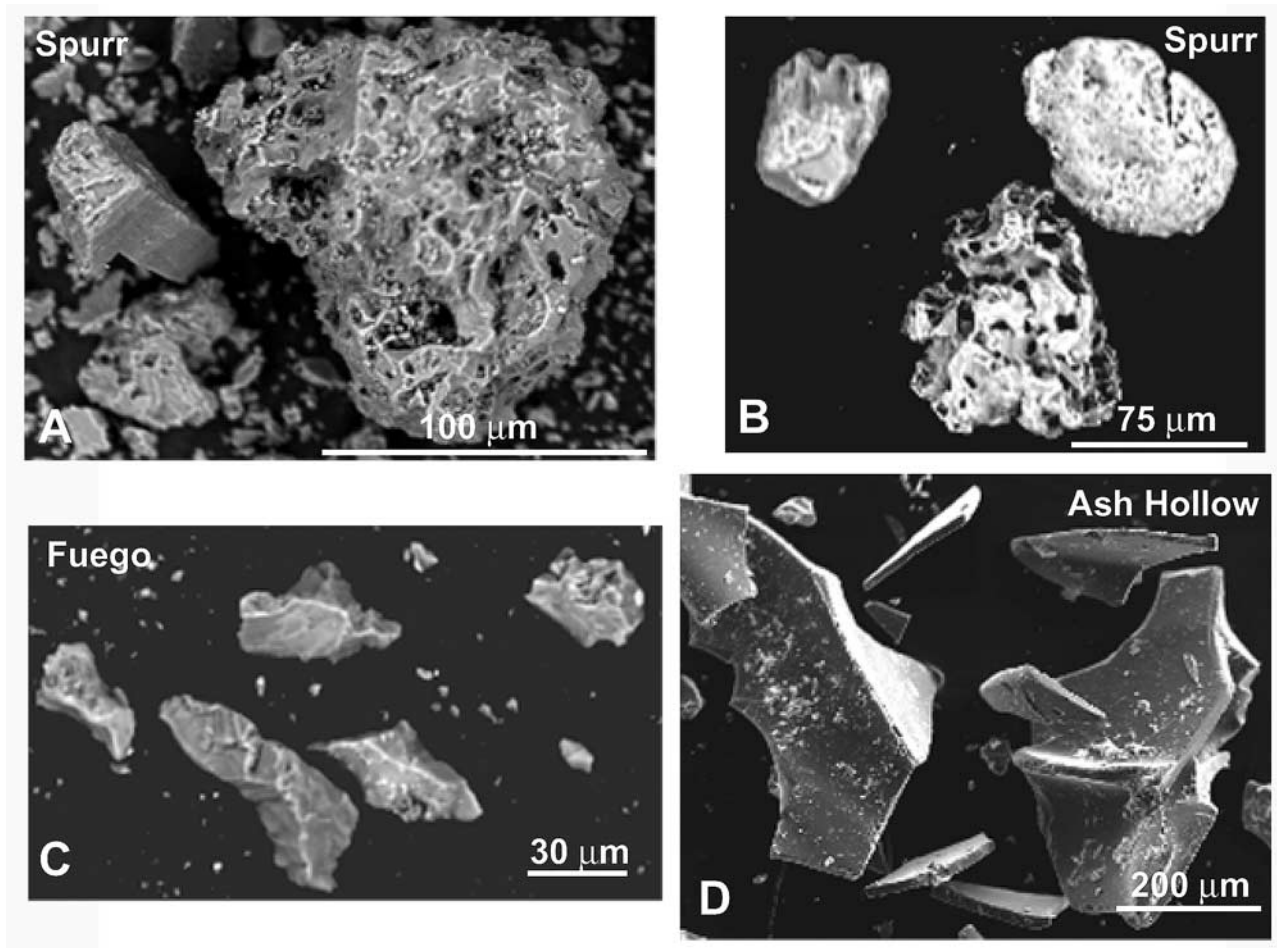
Figure 1. Examples of irregularly shaped ash particles. (a) Equant mineral grain at left and a small pumice clast at right from the August 1992 Spurr eruption. (b) Pumice clasts from the August 1992 Spurr eruption. (c) Angular glass bubble wall shards from the 14 October 1974 Fuego eruption. (d) Bubble wall shards from the Ash Hollow Member ash in Nebraska (Miocene).

particle shape has been made. Numerous qualitative SEM studies (summarized by *Heiken and Wohletz* [1985]) have shown that volcanic particles are generally quite angular and/or irregular and include parachute-shaped bubble wall shards, equant mineral grains, and subrounded vesicular pumice clasts (Figure 1).

[4] Particle shape assumptions in remote sensing retrieval algorithms influence estimates of particle sizes and ash mass concentrations within an eruption cloud [*Mishchenko*, 1993; *Krotkov et al.*, 1997, 1999b]. Both the Total Ozone Mapping Spectrometer (TOMS) and the Advanced Very High Resolution Radiometer (AVHRR), the two most common satellite sensors used to monitor ash clouds, rely on retrieval algorithms for particle size, optical depth, and particle mass concentration. *Wen and Rose* [1994] state that spherical particle shape assumptions in their algorithm result in overestimation of ash mass concentrations in the volcanic cloud. *Krotkov et al.* [1999a] used preliminary andesitic ash results from this study to show that spherical particle shape assumptions in radiative transfer algorithms used to interpret TOMS data underestimate the effective particle radius by as much as 30% and overestimate ash cloud optical depth by as much as 25%. Numerical experiments investigating particles as oblate and prolate spheroids show

scattering by nonspherical particles differs greatly with scan angle, producing both underestimates and overestimates of ash cloud optical depth [*Mishchenko*, 1993; *Krotkov et al.*, 1997].

[5] Ash particle shape is used to determine terminal velocity rates and ashfall distribution for transport modeling. Particle shape affects the velocity with which a particle will fall from the atmosphere [*Stringham et al.*, 1969; *Allen*, 1984] and therefore affects how far a particle will be transported by wind. *Wilson and Huang* [1979] show that the terminal velocities of particles (20–500 μm diameter) can be slowed by orders of magnitude due to particle shape. It is also anticipated that because particle shape affects settling velocities, it should also be accounted for in models of particle reentrainment in eruption columns [*Ernst et al.*, 1996] and in quantitatively assessing the development of settling-driven instabilities in ash clouds [*Holasek et al.*, 1996].

[6] In this study, we characterize the shape and size and determine the terminal velocity of volcanic ash particles for a range of ash compositions. To characterize ash particle shape and size, a methodology which uses air elutriation and image analysis techniques is developed. The data are used to determine which shape, size and compositional
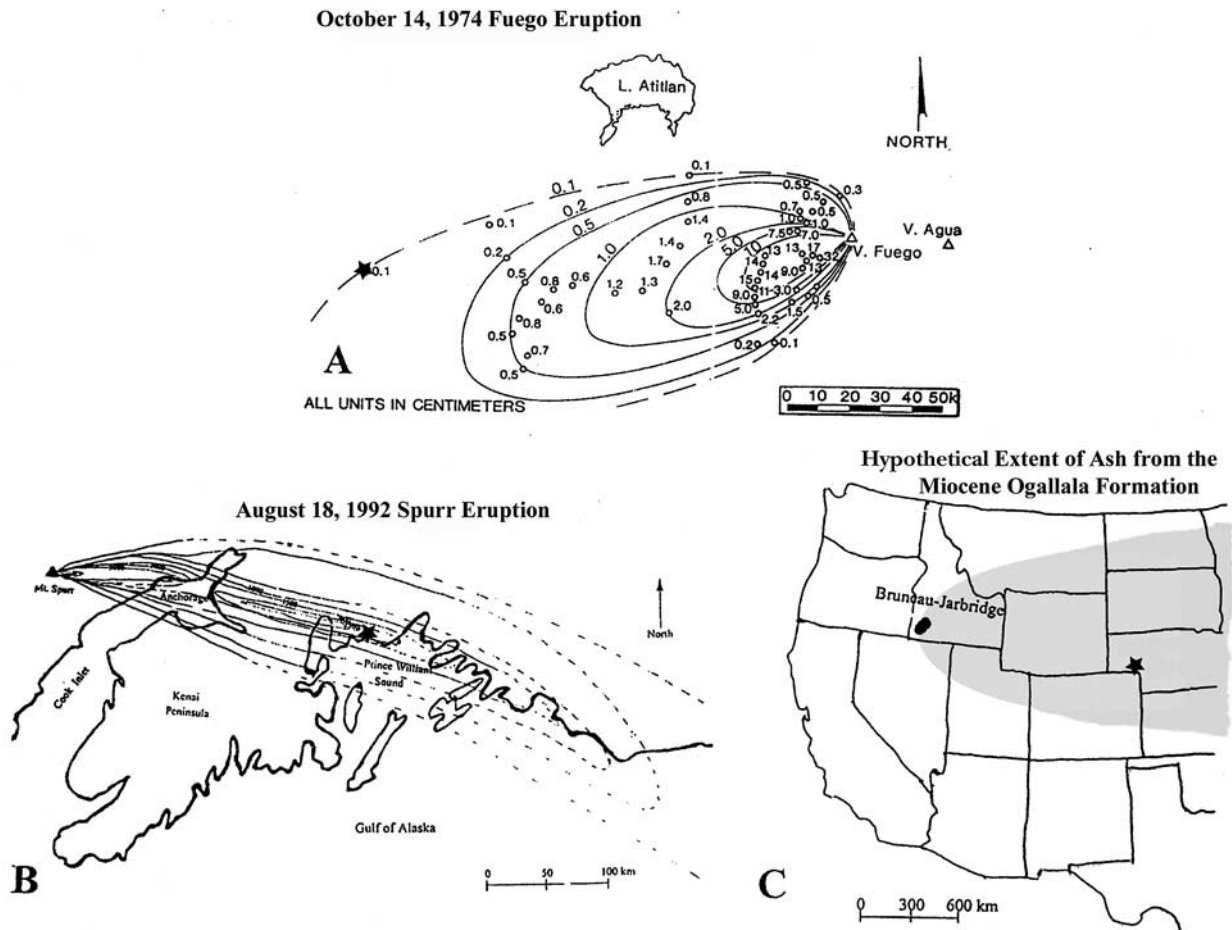
October 14, 1974 Fuego Eruption

Figure 2. Locations of samples used in this study are marked by solid black stars. (a) Isopach map of 14 October 1974 Fuego ash deposit (map courtesy of W. I. Rose). (b) Isomass map of the ash deposits from the August 1992 Spurr eruption showing a secondary maximum ~150 to 340 km from the volcano (map adapted from G. McGimsey, USGS-AVO). (c) Map showing the hypothetical extent of the Miocene Ogallala Formation. The Bruneau-Jarbridge volcanic center may be the source of this ash.

factors are the most valuable descriptors of volcanic ash. Eruption information and sample data for these ashes combined with the particle shape, size, and terminal velocity data from this study provide a basis for future studies that will explore the effects of particle shape using transport models and remote sensing measurements.

2. Eruptions and Ash Samples

2.1. Volcan Fuego, Guatemala

[7] The basaltic 14 October 1974 Fuego ash was produced by a sulfur-rich sub-Plinian eruption that reached a height of 18 km above sea level. The eruption injected 0.03 km^3 dense rock equivalent (DRE) of ash into the atmosphere over a period of 5 hours (W. I. Rose, unpublished data, 2002). The deposit was well sampled with 51 samples collected between 10 and 150 km from the volcano and has been the focus of many studies. Samples were chemically analyzed [*Rose*, 1977; *Rose et al.*, 1978] and grain-size distributions determined [*Murrow et al.*, 1980]. The sample chosen for this study was collected within 48 hours of the eruption (S. B. Bonis, Instituto Geográfico

Nacional, Guatemala City) at a distal location near the edge of the deposit 150 km from the volcano (Figure 2a).

2.2. Mount Spurr, Alaska

[8] The 18 August 1992 Spurr eruption has the most robust data set of the three eruptions in this study [*Rose et al.*, 2001]. The volcanic ash and gas clouds from this eruption were tracked and measured by satellites [*Wen and Rose*, 1994; *Bluth et al.*, 1995; *Schneider et al.*, 1995] and monitored from the ground by radar [*Rose et al.*, 1995] and geophysical observations [*Eichelberger et al.*, 1995]. In addition, over 50 fallout samples were collected within 48 hours following the eruption from 2 to 300 km from the volcano [*Neal et al.*, 1995; *Gardner et al.*, 1998; *McGimsey et al.*, 2001].

[9] The sub-Plinian eruption from the Crater Peak vent at Mount Spurr erupted 14×10^6 m^3 dense rock equivalent (DRE) of pyroclastic material [*Neal et al.*, 1995; *Gardner et al.*, 1998]. The plume reached the stratosphere at a peak altitude of at least 13.7 km above sea level, as detected by radar [*Rose et al.*, 1995], and traveled eastward in the prevailing wind direction [*Schneider et al.*, 1995; *Rose et*
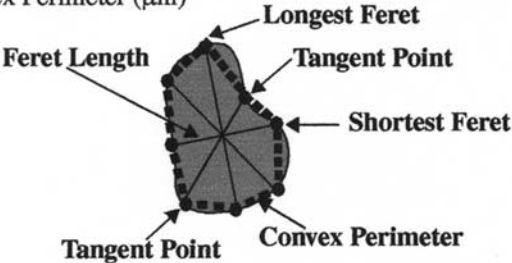
Shape and Size Parameters	Definition
Area (μm^2)	Sum of pixels in an object.
Filled Area (μm^2)	Sum of pixels in an object including holes.
Perimeter (μm)	Sum of pixels making up the object boundary.
Convex Perimeter (μm)	Estimates convex perimeter by adding the pixels making up straight-line distances between feret tangent points along a particle's perimeter. *Feret* length is the distance between two parallel tangents on opposite sides of an object measured at specific angles (see graphic for an example). In this study, 64 ferets were measured for each particle at angles of 5.6° Σ (feret)(2tan[π/2(number of ferets)])
Length (μm)	Longest of 64 ferets measured for an object (see graphic above).
Width (μm)	Shortest of 64 ferets measured for an object (see graphic above).
Aspect Ratio (dimensionless)	Length/Width
Roughness (dimensionless)	Convex Perimeter/Perimeter
Compactness (dimensionless)	4πArea/Convex Perimeter^2
Sphericity (dimensionless)	4πArea/Perimeter^2
Feret Average (μm)	Average length of 64 feret measurements.
Inner Diameter (μm)	Diameter of the largest circle that can fit completely within an object.
Outer Diameter (μm)	Diameter of the smallest circle into which objects can fit completely.
Spherical Diameter (μm)	Estimates the diameter of an equivalent sphere (3-D object). 2 (1.2247)(area/π)$^{1/2}$
Circular Diameter (μm)	Estimates the diameter of an equivalent a circle (2-D object). 2 (area/π)$^{1/2}$
String Length (μm)	Longest measure of diameter assuming object is thin, curved, and elongate. (Perimeter + (Perimeter^2-16(Area))$^{1/2}$)/4
String Width (μm)	Shortest measure of diameter assuming object is thin, curved, and elongate. (Perimeter - (Perimeter^2-16(Area))$^{1/2}$)/4
X-Projection (μm)	Sum of pixels between the vertical intercepts of a particle divided by 2.
Y-Projection (μm)	Sum of pixels between the horizontal intercepts of a particle divided by 2.

Figure 3.   Image analysis measurement definitions.

al., 2001]. A bulk deposit isomass map (Figure 2b) for this eruption shows that the tephra deposit contains an area of secondary thickening ∼200 km away from the volcanic source [*McGimsey et al.*, 2001].

[10] The sample used in this study was collected approximately 225 km ESE of Spurr near Wells Bay [*McGimsey et al.*, 2001]. The ash was deposited in this area 7–8 hours after the start of the eruption based on reports and observations of ash falling in nearby areas [*Eichelberger et al.*, 1995].

2.3. Ash Hollow Member, Nebraska

[11] The late Miocene (9–11 Ma) Ogallala Formation contains at least ten ash members which extend from Nebraska to Texas, covering thousands of square kilometers [*Frye et al.*, 1995]. The Ash Hollow Member is the topmost ash unit of the Ogallala Formation and is of rhyolitic composition [*Swinehart et al.*, 1985]. The source of this ash is unknown (Figure 2c), but the formation age corresponds to the time of activity of the Bruneau-Jarbridge center of the Snake River Plain [*Perkins et al.*, 1995; M. E. Perkins, personal communication, 2001]. The distribution of this ash deposit (Figure 2c) is difficult to map since the ash was partially redistributed by wind and water into deposit thicknesses of up to 22 m [*Swinehart et al.*, 1985], and the multiple ash layers deposited in this area require chemical analyses in order to trace separate ash layers (M. E. Perkins, personal communication, 2001). The ash extent shown in Figure 2c is only an estimate of where ash may have been deposited if erupted from the Bruneau-Jarbridge center.

[12] The ash sample used in this study was collected from the Ash Hollow member in southwestern Nebraska near Broadwater where it is ∼1m thick and overlies a 2.5–3 m thick conglomerate. The sample was collected 40–70 cm from the top of the deposit where the ash is laminated (1–2 cm thick layers) and where there was a layer of accretionary lapilli that individually measured 5–7 mm in diameter. The sampled outcrop showed the least fluvial influence of all the outcrops sampled, and the ash particles showed few effects from weathering.

3. Methods

[13] Grain-size distributions for the bulk samples of all three ashes were measured by Malvern Instruments Ltd. using the Malvern Mastersizer 2000 laser diffraction instrument (Appendix A, Appendices A–M are available as auxiliary material)[1] (Malvern Instruments Ltd., Laser diffraction for particle size analysis-why use Mie theory?, LabPlus International, Malvern, U.K., 2000, available at http://www.malvern.co.uk; A. Rawle, Basic principles of particle size analysis and Malvern sizes up the industry with laser diffraction techniques, Laboratory Equipment, technical papers, Malvern Instruments Ltd., Malvern, U.K., 2000, available at http://www.malvern.co.uk). An air elutriation device called the Roller particle size analyzer (Appendix B) [*Roller*, 1931a, 1931b] was used to sort the ash samples into terminal velocity groups. The air flow rates used to sort the

samples were incorporated into the Stoke's law equation (since airflow through the Roller analyzer is laminar) and terminal velocities were determined for the sorted groups (Appendix C). While sorting the sample some of the particles in the lowest three terminal velocity groups (0.6–3.7 cm/s) clumped together to form aggregates (Appendix D), which may introduce some error in the shape measurements. The ash particles in each terminal velocity group were applied to aluminum stubs for use with the scanning electron microscope (Appendix E). Two to seven backscattered images containing totals of 27 to 145 individual particles were collected for each terminal velocity group using a Jeol JXA-8600 electron microprobe analyzer (Appendix F). Bit maps were made of the particles in each image and shape and size measurements (Figure 3) were made by an automated image analysis program called Clemex Vision™ (Appendix F). Surface areas for bulk samples of the three ashes were also made using the BET (Brunauer, Emmett, and Teller) method (Appendix G) [*Brunauer*, 1945].

4. Results
4.1. Physical Description of Particles
4.1.1. Fuego

[14] A total of 1300 particles were measured by SEM imagery in the various Roller splits for the Fuego sample (Figure 4a) and categorized as (1) vesicular, (2) nonvesicular, and (3) miscellaneous particles (Appendix H). The bulk of the Fuego sample is composed of nonvesicular glass (75%), perhaps containing microphenocrysts. The rest of the sample is composed of basaltic pumice clasts (25%) having 38% vesicles, and trace amounts of other particles that could not be identified (Appendix H). Previous studies [*Rose et al.*, 1978] have shown that coarser juvenile particles (>200 μm) in the Fuego fall deposits contain 38% phenocrysts, including olivine, magnetite, augite, and amphibole. These phenocrysts are typically far larger than 200 μm in diameter and are rare or absent in the fine-grained fall sample studied here. Both vesicular and nonvesicular particles have a high electron beam reflectance in backscatter images and so appear bright in the images (Figure 4a).

4.1.2. Mount Spurr

[15] Approximately 1300 particles were measured for the 18 August 1992 Spurr fallout sample (Figure 4b). The majority of the vesicular particles are andesitic pumice clasts that have 20–40% vesicles. These vesicular clasts are generally larger than the nonvesicular particles (perhaps because the nonvesicular particles are fragments of the larger vesicular clasts) and gray or tan in color. Images of the vesicular particles show that they contain small crystals, called microlites, of plagioclase and pyroxene [*Gardner et al.*, 1998]. The majority of nonvesicular particles are glass bubble wall shards with microlites, and make up 44% of all the measured particles. Trace amounts of "other" particles, probably mineral ("dust") grains, were measured, but due to the rarity of these particles are considered environmental contaminants (Appendix H) and ignored in this study.

4.1.3. Ash Hollow

[16] Over 850 particles were measured for the Ash Hollow sample (Figure 4c). The sample is composed almost

---

[1] Supporting appendices are available at ftp://agu.org/apend/jb/ 2001JB00818.
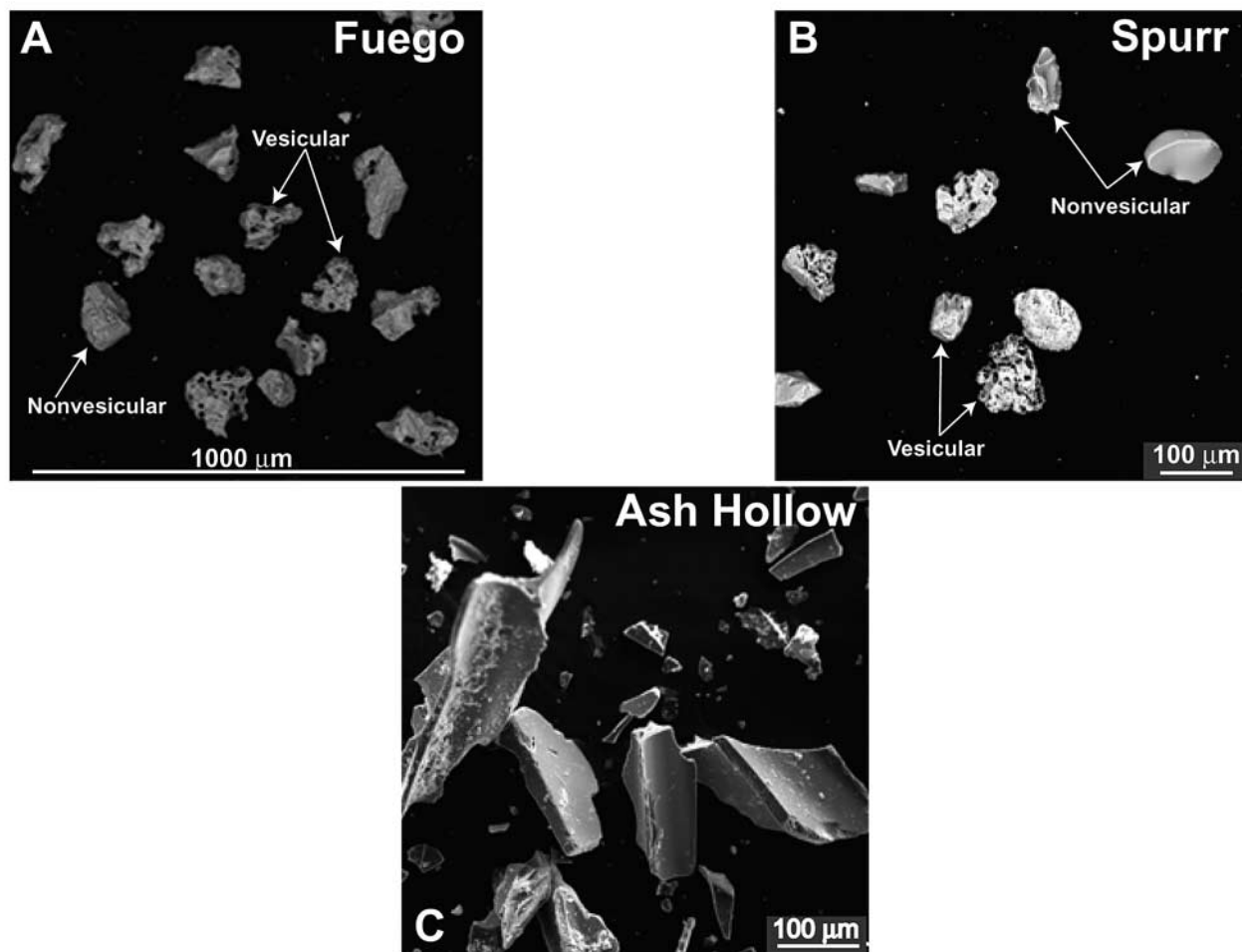
Figure 4. SEM images showing typical particle types (vesicular and nonvesicular) and shapes observed in the ashes studied. (a) Vesicular and nonvesicular basaltic clasts in Fuego ash. (b) Vesicular pumice clasts and nonvesicular glass shards in andesitic ash from Spurr. (c) Bubble wall shards from the rhyolitic ash of the Ash Hollow Member, Nebraska.

totally of bubble wall shards (>99%) and has no pumice clasts (Appendix H). The glass shards are platy and have small thicknesses (~20 μm) compared to their widths (~110–140 μm) and often show distinct bubble junctions and bubble wall curvatures. No phenocrysts were observed within the glass or as individual particles.

4.2. Chemical Composition of Particles

[17] Appendix I shows compositional data and references which give detailed information on the three ashes studied. The 1974 Fuego magma is a high-aluminum basalt with substantial phenocryst content (W. I. Rose, unpublished data, 2002). The sample studied is distal (~150 km from the volcano) and reflects preferential fallout of large phenocrysts. The Spurr magma is calcalkalic andesite with a slightly lower crystal content than Fuego [*Gardner et al.*, 1998]. The sample studied is distal (~250 km from the volcano) and has probably also lost most or all of its phenocrysts in near-source fallout. Both Fuego and Spurr have hypocrystalline to hyalocrystalline groundmass components [*Gardner et al.*, 1998; W. I. Rose, unpublished data, 2002], which are the dominant components of the ashes

studied. The Ash Hollow sample is composed completely of homogenous hydrated rhyolitic glass.

4.3. Grain-Size Distribution Results

[18] Grain-size distribution results for the Fuego sample (Figure 5a) show the sample is unimodal, poorly sorted according to sedimentological standards (though is well sorted as compared to most volcanic ash samples), and has a high skewness, indicating that a high proportion of the sample is within the fine-grained tail (Table 1). This is contrary to a previous study which obtained less detailed grain-size data on the same ash sample using Coulter counter and sieves [*Murrow et al.*, 1980] and showed a weakly bimodal distribution. The change in measurement devices for coarse and fine particles in that study probably introduced some error which made the sample look bimodal. The precise measurements and range of sizes that laser diffraction devices can measure (0–2000 μm) make their data superior to the older sieve and Coulter counter methods.

[19] The grain-size distribution of the Spurr sample, as indicated by laser diffraction methods, is bimodal (Figure 5b)
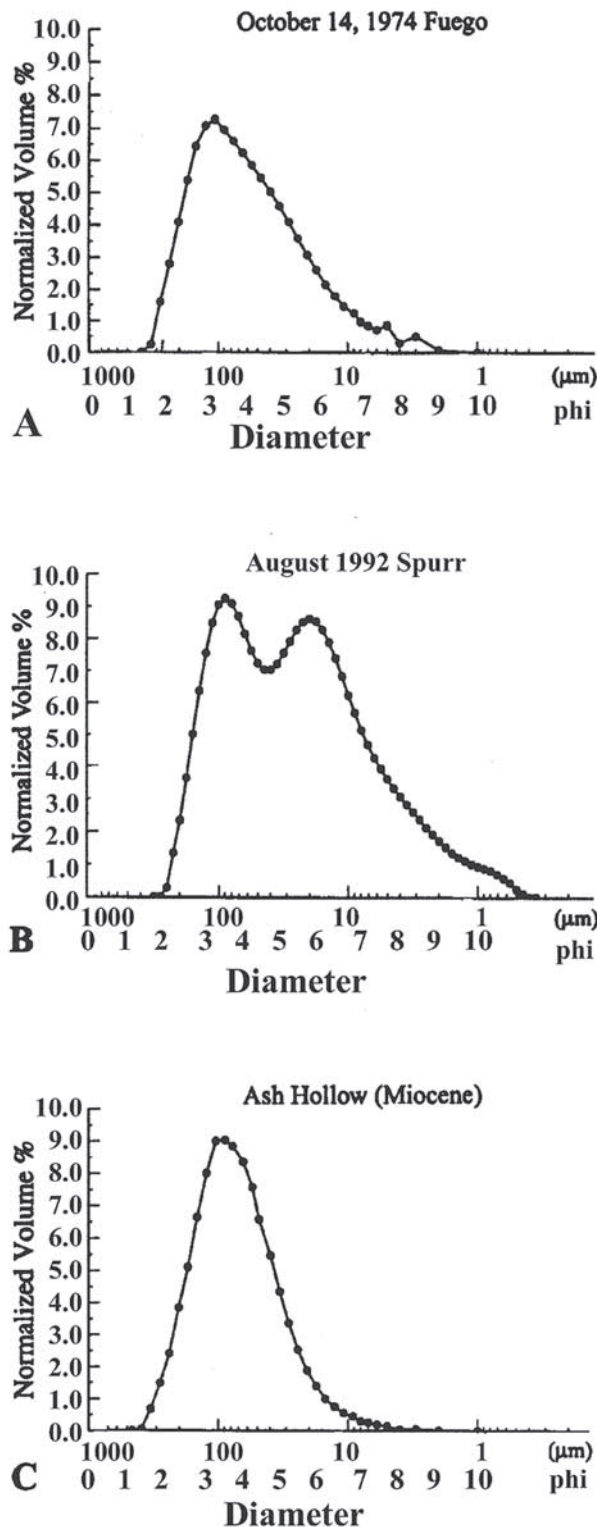
Figure 5. Grain-size distributions determined by laser diffraction. (a) The Fuego, (b) Spurr, and (c) Ash Hollow Member ash samples are all sedimentologically poorly sorted and rich in fines. The Spurr sample has a distint bimodal distribution. Grain-size values below 10 μm become increasingly inaccurate with decreasing size due to limitations in the laser diffraction method.

Table 1. Grain-Size Characteristics of Ash Samples

	Md[a]			
Sample	ϕ	Microns	σ_ϕ	α_ϕ
Fuego	4.9	33.5	1.34	+1.05
Spurr	5.3	25.0	1.78	+0.42
Ash Hollow	3.7	76.9	1.07	+0.38

[a]Md is the median grain-size diameter for an ash particle.

with peaks at 3.5 and 5.5ϕ (88 and 22 μm). The sample is sedimentologically poorly sorted and has a prominent fine tail (Table 1). Grain-size distribution results for the Ash Hollow sample (Figure 5c) show that the sample is unimodal, sedimentologically poorly sorted, and rich in fine particles <100 μm in diameter (Table 1).

4.4. Quantitative Shape Measurements

[20] All the particle shape and size results are listed in Appendices J–L and summarized in Table 2. The various parameters measured for each particle are tabulated in measurement categories of shape and size. Data for individual particles were separated into nonvesicular and vesicular particle groups for the Fuego and Spurr samples. By separating the particles into groups, we aim to provide greater detail on how particle shape and size affect terminal velocity versus using group means. Three types of means were calculated for each parameter in each terminal velocity group: (1) a combined mean which uses measurement data from both nonvesicular and vesicular particle types, (2) a vesicular mean, and (3) a nonvesicular mean. Combined, vesicular, and nonvesicular means for shape and size parameter measurements are given in Appendix J for Fuego and Appendix K for Spurr. The Ash Hollow, NE sample only contained nonvesicular particles (Appendix L).

4.5. Image Processing Measurements

[21] The pattern observed for the shape parameter feret average (the average of 64 diameter measurements for a single particle; Figure 3) is similar to patterns observed for perimeter, length, and area, and shows that measurements increase in parabolic fashion with increasing terminal velocity in all ash samples (Figure 6a). For all these parameters, Ash Hollow measurements plot above Spurr and Fuego, reflecting their more complex shape. The pattern observed in aspect ratio data is (Figure 6b) flat for Spurr and Fuego, but varies for Ash Hollow. Ash Hollow values are usually higher than Spurr and Fuego values. Results for sphericity and roughness do not have clear patterns with increasing terminal velocity, though values are constrained between 0.6–0.8 for sphericity and 0.9–1.0 for roughness in all ash samples.

[22] Figure 7 compares measured terminal velocities of some of the size parameters to calculated terminal velocities assuming a spherical shape. Generally, the curves are steeper for smaller particles and flatten as the size of particles increase. Measured diameters at specific terminal velocities for Ash Hollow are larger than those for Spurr and Fuego.

4.6. Nonvesicular and Vesicular Mean Results

[23] Nonvesicular and vesicular means were compared for Fuego (Figure 8) and Spurr (Figure 9) samples. The Ash

Table 2. Summary of Selected Shape Data

	Fuego	Spurr	Ash Hollow
TV = 1.3 cm/s			
Feret average, μm	15	12	21
Aspect ratio	1.7	1.5	1.8
Perimeter, μm	47	38	66
Convex perimeter, μm	45	36	65
TV = 7.3 cm/s			
Feret average, μm	40	45	60
Aspect ratio	1.6	1.5	2.1
Perimeter, μm	135	145	240
Convex perimeter, μm	130	140	180
TV = 18.0 cm/s			
Feret average, μm	80	90	90
Aspect ratio	1.5	1.4	2.5
Perimeter, μm	265	290	300
Convex perimeter, μm	245	280	290
TV = 43.1 cm/s			
Feret average, μm	110	120	
Aspect ratio	1.5	1.5	
Perimeter, μm	365	380	
Convex perimeter, μm	345	370	
BET surface area, m²/g	0.7919	1.0059	1.2291
Calculated surface area,[a] m²/g	0.06	0.14	0.03

[a]Calculated using surface area equation for a sphere and feret diameter.

Hollow sample contained only nonvesicular particles. Patterns for feret average (Figures 8 and 9a) are similar to those for area, perimeter, and length and show that vesicular particles generally have higher mean values than nonvesicular particles except for the lower terminal velocity groups of Fuego (TV < 18 cm/s). The Fuego curves do not show as much variability between nonvesicular and vesicular particles within individual TV groups as Spurr. The differences between vesicular and nonvesicular values in all curves for both Fuego and Spurr samples become greater as terminal velocity increases.

[24] Nonvesicular fractions of both ash samples generally show higher values of aspect ratio (Figures 8 and 9b), compactness, sphericity, and roughness than vesicular fractions. For aspect ratio, both the Spurr and Fuego samples have more variability in their highest velocity groups.

4.7. BET Surface Area Results

[25] BET surface area results are (Table 2) up to 100 times greater than those calculated for surface areas of various geometrical shapes (Figure 10) using our measurements for feret average, length, and width. Even the more reasonable surface area calculations (using cylinders for Fuego and Spurr and a disk for Ash Hollow) which lie closest to the BET values only account for 30 to 50% of the surface area of the ash.

5. Discussion

[26] We have described shape and size measurements from Spurr, Fuego, and Ash Hollow samples with the goal of explaining how ash particle shape influences terminal velocity and remote sensing radiance measurements. We have generated numerical results and will now investigate how we can use them.

[27] The basic data we have generated, without any further calculations or manipulations, are profound in their statements about particle shape in volcanic fallout.

[28] 1. The ash sample that traveled the greatest distance, Ash Hollow, contains the coarsest particles (Table 1). Although it is clear from the huge inferred extent of the Ash Hollow airfall that it corresponds to an eruption of much higher intensity (and column height) than either the Fuego or Spurr cases, it is still surprising that the Ash Hollow deposit is so coarse at ~1200 km from the source. This highlights that particle size (with wind speed and column height accounted for) is inadequate to characterize ash dispersal and model it. Particle shape can play as important a role as these
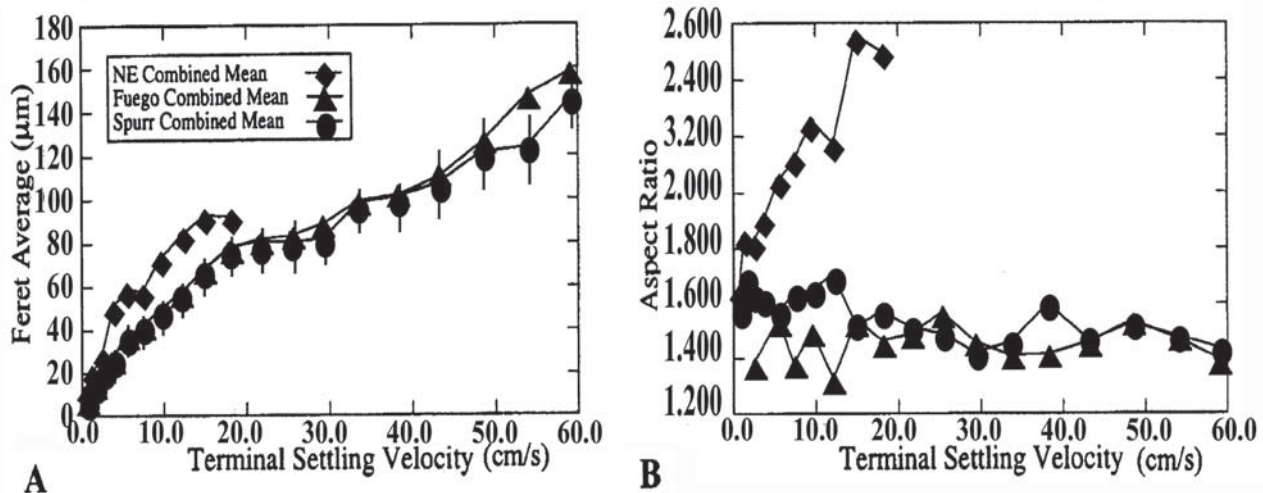

Figure 6. Shape and size parameters compared with terminal velocity for all three ash compositions. Values are combined means (measurements for both pumice and glass particle types are used). (a) Error bars show the standard deviation of the combined mean and would have similar relative values in other shape and size parameter graphs. The feret averages for Fuego and Spurr are similar, but Ash Hollow (NE) ash has a different pattern. (b) Aspect ratios for all ashes differ greatly from the value (1.0) typically assumed for spherical particles. See Figure 3 for definitions of the different shape and size parameters.
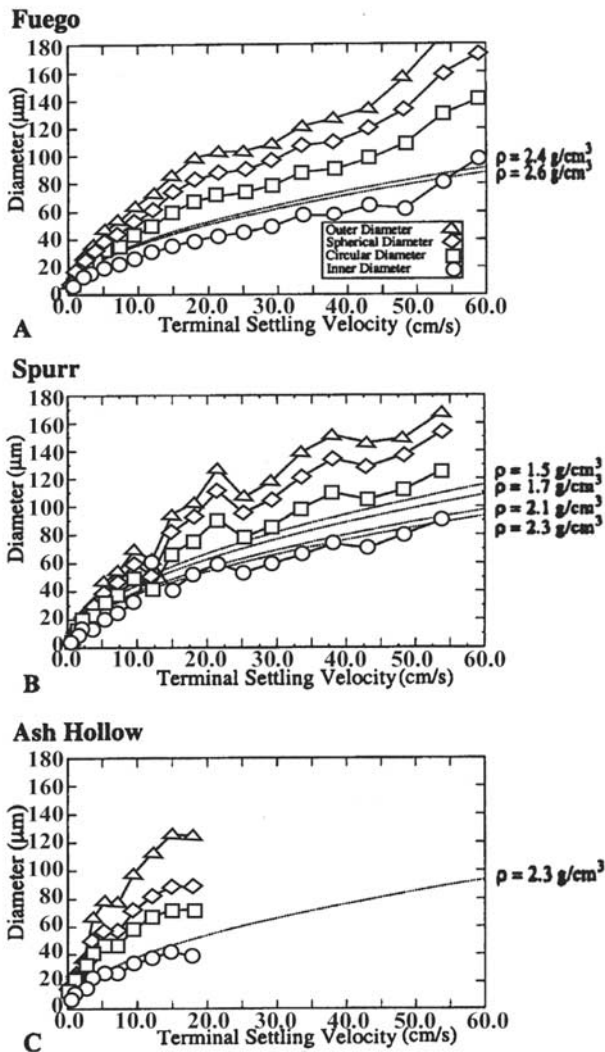
Fuego

Spurr

Ash Hollow

Figure 7. Comparison of measured terminal velocities to terminal velocities calculated for spheres of the appropriate densities (1.5, 1.7, 2.1, 2.3 g/cm^3 for Spurr; 2.4 and 2.6 g/cm^3 for Fuego; and 2.3 g/cm^3 for Ash Hollow). Values are combined means. All diameter measurements except "inner diameter" are much larger than diameter values predicted for spherical particles at the same terminal velocities. See Figure 3 for definitions of the different diameter measurements.

other factors and should be carefully considered in future studies.

[29]   2. At identical terminal velocities the three ash samples studied vary markedly in density, area, perimeter, length, width, feret average, aspect ratio, and compactness. This shows that we can measure highly variable shape aspects.

[30]   3. The extreme difference between measured and calculated surface areas combined with SEM observations of the ash samples indicate that there is a significant surface area contribution from fine scale roughness, porosity, and the irregular shapes of volcanic ash which is likely to significantly affect chemical processes, electrostatic

aggregation, and scattering phenomena in the volcanic cloud.

5.1.   Which Image Processing Measurements Are Most Useful for Predicting Terminal Velocity?

[31]   The relationship between particle shape and drag is not well understood, despite many experimental and theoretical studies. Most studies have focused on coarse particles with simple geometrical shapes (spheres, disks, cubes, prolate spheroids, oblate spheroids, etc.) [e.g., *Pettyjohn and Christiansen*, 1948; *McNown and Malaika*, 1950; *Jayaweera and Mason*, 1965; *Stringham et al.*, 1969; *Allen*, 1984]. A few experiments measured the actual settling rates of irregular-shaped volcanic and sedimentary particles [*Fisher*, 1964; *Walker et al.*, 1971; *Komar and Reimers*, 1978; *Wilson and Huang*, 1979]. *Walker et al.* [1971] measured terminal velocities of various pyroclasts and showed that their fallout rates were similar to theoretically determined terminal velocities for cylinders. *Wilson and Huang* [1979] measured the terminal velocity of glass, pumice, and feldspar particles (30–500 μm) from ashfall materials. They also measured each particle's diameter along three axes and found differences of orders of magnitude in terminal velocity related to particle shape and atmospheric drag.

[32]   In this study, particles are characterized by a wide range of shape and size parameters and their terminal velocities are directly measured. The most useful measured parameters found by this study for predicting terminal velocity are believed to be the feret average, aspect ratio, sphericity, and roughness (see Figure 3 and Table 2).

5.2.   Which Shape Parameters Are the Best Shape Descriptors?

[33]   The difference between the three ashes studied is shown clearly by the aspect ratio and feret average (Figure 6). The Spurr and Fuego samples show similar size and shape trends overall which matches their visual similarity (Figures 4a and 4b), but the Ash Hollow sample is dramatically different (Figure 4c), having a much steeper increase in measured values with increasing terminal velocity and higher values than the other two ashes.

[34]   For remote sensing applications, we have been able to use the aspect ratio data to improve calculations for effective radius and volcanic cloud mass concentrations [see *Krotkov et al.*, 1999b]. The aspect ratio tells us about the shape and surface area of a particle. The wide variability in aspect ratios measured for nonvesicular particles of the Ash Hollow sample, and low terminal velocity particles in the Spurr and Fuego samples, suggest that these particles have shapes whose form is greatly influenced by relict bubble walls (fragmentation by expanding gases in the magma would cause breakage along irregularly distributed vesicles and concave-shaped bubble walls).

[35]   For the estimation of surface area, the best descriptors may be perimeter and convex perimeter, which are used to determine sphericity, compactness, and roughness (Figure 3). The surface area of ash is important in issues of charging and aggregation [*Lane and Gilbert*, 1992; *Gilbert and Lane*, 1994] and also in the kinetics of heterogeneous chemical reactions such as the conversion
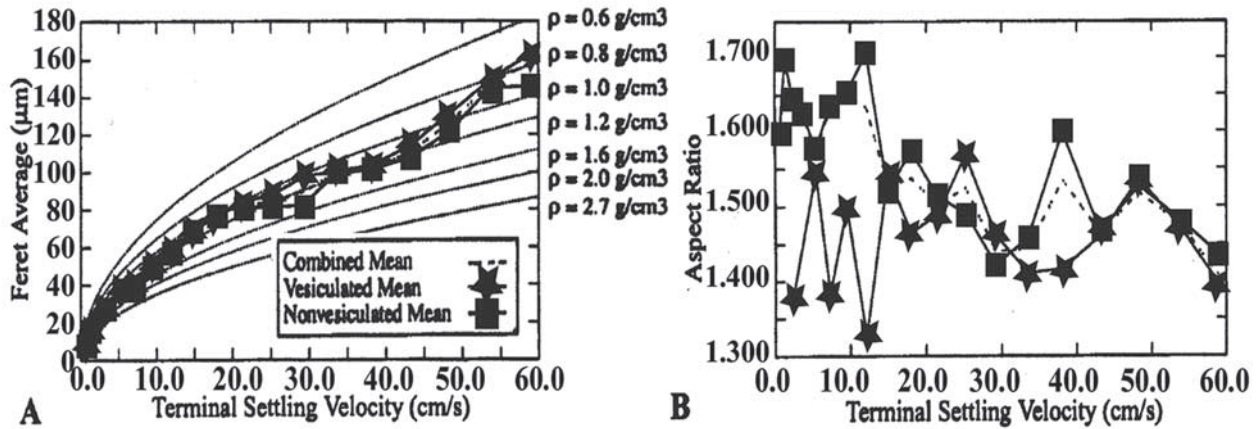
Figure 8. Shape and size parameters compared to terminal velocity for the combined, vesicular, and nonvesicular mean values of particles in Fuego ash. Density curves for spherical particles are plotted for feret average to assess density influences on terminal velocity. (a) Feret average shows that most vesicular particles have larger values than nonvesicular particles at similar terminal velocities. (b) Aspect ratio shows that nonvesicular particles have higher values than vesicular particles at similar terminal velocities.

of SO_2 to sulfate [*Schneider et al.*, 1999]. Surface area is also important to particle fallout since more surface area means greater contact with the atmosphere which produces greater drag, resulting in greater transport distance from the source (for a given eruption intensity). Since the perimeter and convex perimeter values are similar, the sphericity and compactness measurements do not differ greatly. If the particles had greater changes in their surface topography (greater roughness), sphericity and compactness values would be more distinct. These measurements show the Ash Hollow particles have the greatest surface area.

[36] Figure 11 compares the measured perimeters for all ashes to the calculated equivalent perimeters of spheres at the same terminal velocity. The measured perimeters are 1.5 to 2 times larger than calculated perimeters.

5.3. How Can Image Processing Measurements Be Used to Predict Surface Area?

[37] The surface area of a sphere is easily related to the diameter by πd^2, so the feret average can be used as "diameter" to convert to an equivalent spherical surface area, which will always be less than the real surface area (sphere density is assumed to equal the same density as the volcanic ash composition). Surface areas calculated by this method for the ash samples were shown in Figure 10. The comparison of these calculated surface areas to BET derived surface areas showed the calculated surface areas were
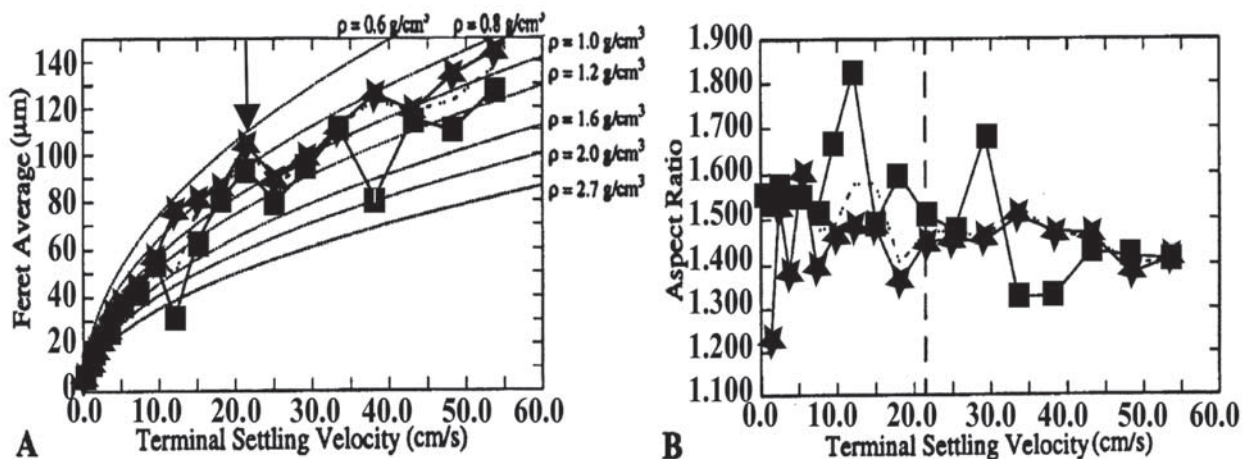

Figure 9. Shape and size parameters compared to terminal velocity for the combined, vesicular, and nonvesicular mean values of particles in Spurr ash. The arrow in Figure 9a denotes the TV = 21.5 cm/s peak found in some diagrams (see text). The vertical dashed line in Figure 9b marks the change in shape parameter values which may be related to changes in fragmentation mechanisms.
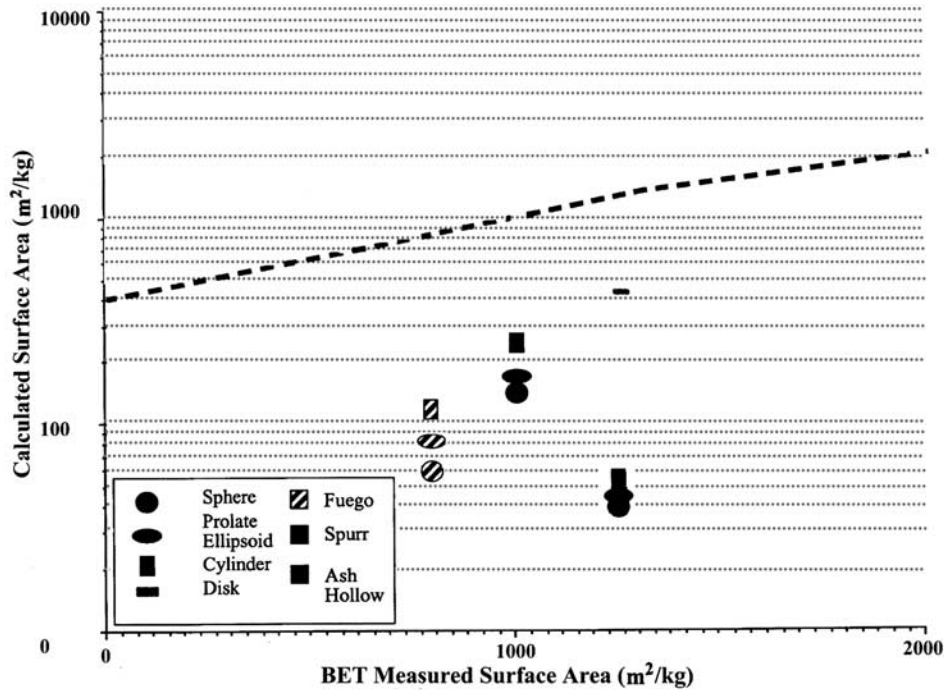
Figure 10. BET (Brunauer, Emmett, and Teller method) surface area compared to calculated surface area for various geometrical shapes. Calculated surface areas were derived using image analysis measurements for radius (r), width (w), length (l), and thickness (t) (for cylinders, r is feret average and l is length; for ellipse, l is length, w is width, r is feret average; for sphere, r is feret average; and for disk, $t = 20$ μm, r is feret average) and total grain-size distributions of the deposits. The dashed line represents equal values of calculated surface area and measured surface area (1:1 ratio).

substantially lower by a factor of 1 to 2. The "missing" surface area comes from particle porosity, fine roughness, and the irregular shapes of particles which cannot be described completely by simple geometric shapes or two-dimensional image analysis methods. The calculation for surface area of the Ash Hollow sample was greatly improved by using a disk to represent the shapes of the thin glass shards. This also emphasizes the importance of particle shape in surface area calculations.

[38] It would be useful to have a factor which would adjust the calculated surface area values to reflect the true surface areas as determined by BET analysis. Such a correction factor (F) for spheres (the shape most commonly used by modelers) of a specific composition can be determined using the ratio of BET surface area to calculated surface area assuming spherical shape (Table 3).
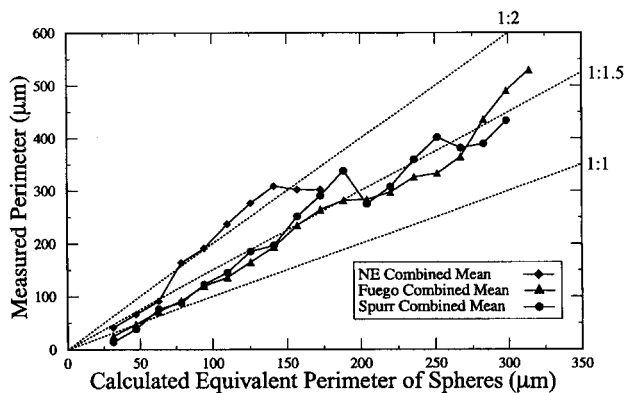

Figure 11. Measured perimeter compared to the calculated perimeter of spheres that would fall out at the same settling velocity. Dotted lines represent ratios of calculated perimeters to measured perimeters.
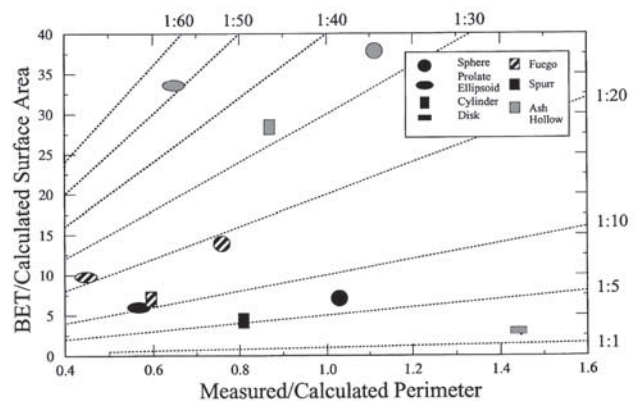

Figure 12. Surface area compared to perimeter for various geometrical shapes. All calculated values of surface area and perimeter were derived using the image analysis measurements of feret average, width, and length. The dotted lines represent ratios of BET/calculated surface areas to measured/calculated perimeters.

Table 3. Calculated Surface Areas Using Correction Factors and Different Grain Size Distribution Determinations

		Surface Area		
	Correction Factor F[a]	BET, m²/g	Corrected Laser Diffraction,[b] m²/g	Corrected Sieve and Coulter Counter,[b] m²/g
Fuego	14	0.7919	1.0	1.9
Spurr	7	1.0059	1.6	na
Ash Hollow	38	1.2291	1.7	na

[a]F = BET surface area divided by calculated surface area from grain-size data.
[b]Calculated surface area from grain-size data multiplied by the correction factor; na, not available.

[39] The correction factors were tested by using the particle radii (r) from laser diffraction grain-size distributions and Coulter counter/sieve measurements of the ash samples. Perimeters of spherical particles ($2\pi r$) were calculated and surface areas ($2r \times$ perimeter) determined for each particle. The total calculated surface area was multiplied by the correction factor most appropriate for the ash composition used (Table 3). Surface area results were within a factor of two or better to the values determined using BET analysis. The corrected surface area for Fuego using sieve and Coulter counter data greatly overestimated surface area, whereas, the Mastersizer results were much closer to the BET value, which emphasizes the importance of obtaining detailed and accurate grain-size data.

[40] The surface area ratios are much greater than the perimeter ratios, especially for the Ash Hollow sample (Figure 12). This emphasizes that the irregular shapes of ash particles are not accurately described by 2-D measurements like perimeter. The simple geometric shapes used are poor descriptors of the real particle shapes. The disk used for Ash Hollow was closest to the BET measured values.

5.4. Which Particle Size Measurements Are the Most Useful?

[41] Many methods of shape classification have been developed which use particle diameter [*Wadell*, 1932; *Zingg*, 1935; *Corey*, 1949]. These methods were considered by *Wilson and Huang* [1979], who describe particle shape using the shape factor, SF,

$$SF = (b + c)/2a$$

where a, b, and c represent the longest, intermediate, and short particle axes, respectively.

[42] We used the values for feret diameter to determine the *Wilson and Huang* [1979] shape factor, F, since this factor has been used in several transport models [*Suzuki*, 1983; *Glaze and Self*, 1991; *Center for Nuclear Waste Regulatory Analyses*, 1997]. The values used for long, intermediate, and short axes are length, feret average, and width, respectively. Our results show that the shape factor is 0.7–0.8 for Fuego and Spurr and 0.6–0.7 for Ash Hollow (see Appendices J–L). This compares to a shape factor value of 0.5 which was determined by *Wilson and Huang* [1979] for the volcanic particles they studied (rhyolite ash from the Toba eruption).

[43] In order to determine how particle shape affects fallout, density influences need to be separated from

shape influences. The terminal velocities of perfect spheres were compared at various densities with the ash size data (Figures 7, 8a, and 9a).

[44] Measurements of Spurr pumice densities were made by *Gardner et al.* [1998] using the *Hoblitt and Harmon* [1993] method on ash deposited near the volcanic source (<15 km). These deposits contain two types of pumice clasts that differ in density, vesicularity, and color but not in chemical composition [*Neal et al.*, 1995]. Tan pumice clasts are found at the bottom of the deposit and grade to gray pumice clasts at the top of the deposit [*Neal et al.*, 1995]. *Gardner et al.* [1998] determined that the tan pumice clasts had densities of 1.5–1.7 g/cm³ and that the gray pumice clasts had densities of 2.1–2.3 g/cm³. The Spurr ash sample used in this study contained both tan and gray pumice clasts, so we compared the data to density curves based on both of Gardner's estimates (Figures 7b and 9a).

[45] The bulk density of the Fuego ashfall has been estimated in the field at 1.14 g/cm³ (W. I. Rose, unpublished data, 2002). The density of individual ash particles is much higher than this estimate, however. The sample contains both nonvesicular and vesicular clasts, so we compared the shape measurements to density curves (Figures 7a and 8a) using a density of 2.4–2.6 g/cm³ for the nonvesicular basalt clasts [*Fisher*, 1964; *Brazier et al.*, 1982]. Particle density for Ash Hollow particles (Figure 7c) has not been precisely determined, but the particles are nonvesicular and so their density is assumed to approximate rhyolitic glass (2.3 g/cm³ [*Williams et al.*, 1954]).

[46] Our measurements (Figures 7, 8a, and 9a) show that particles are falling out at slower velocities than predicted by the density curves, indicating that particle shape greatly increases drag. Extrapolation of the appropriate density curves indicates large particles are falling out at terminal velocities that are slower by factors of up to 10 or more. The shape and drag affects all three ash samples, becomes more marked for larger particles, and is greatest for the Ash Hollow sample which is the ash with the most extreme aspect ratio.

[47] Another way to consider shape effects on fall velocity is to calculate the diameter of perfect spherical particles that would fall at the same terminal velocity as the ash
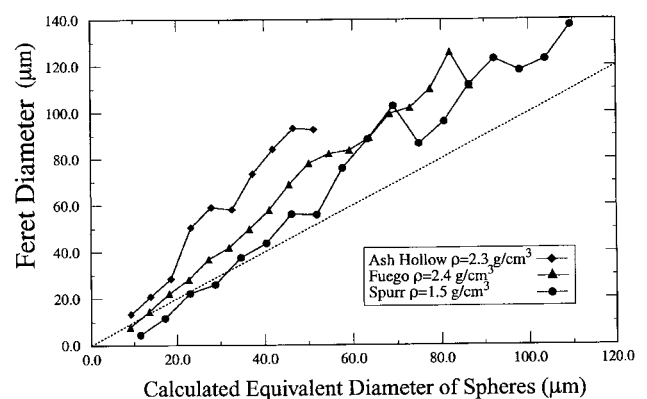
Figure 13. Feret diameter compared to the calculated diameter of spheres that would fall out at the same settling velocity.

particle groups (tabulated in Appendix M). These diameters are plotted in Figure 13 and compared to feret averages for the three ash samples studied. Data show that the feret averages are much greater than ideal spherical particle diameters, indicating that shape causes particles to fall at a considerably slower rate. Feret diameters in the lowest velocity groups are smaller than the spherical particles for Spurr and Fuego. These results are probably due to aggregation in the settling chamber which would cause the small particles (as part of an aggregate) to fall out at higher terminal velocities than they would normally have if they were traveling individually. This hypothesis is supported by the collection of aggregates in the settling chamber at low flow rates.

5.5. How Are the Shapes of Spurr Particles Affected by Vesicles and Phenocrysts?

[48] During our analysis of the particle measurements area, perimeter, feret average (Figure 9a), and various other diameters (Figure 7b), we noticed that the combined mean curves for Spurr had unusual peaks at TV = 21.5 cm/s and TV = 38.1 cm/s. These have equivalent feret averages of ~100 μm and 125 μm. The peak at TV = 38.1 cm/s is most likely statistical, reflecting the small number of nonvesicular particles measured in this group (<10%; Appendix H), resulting in large error for the nonvesicular mean. The peak at TV = 21.5 cm/s is not statistical, since >17% of the particles measured were nonvesicular. We ruled out experimental factors for this peak since it does not correlate to any changes in flow rate, chamber diameter, or nozzle size, and the collection procedure was the same as for other settling groups (Appendix B). The peak may reflect fragmentation mechanisms controlled by the size, density and geometry of vesicles and phenocrysts in the magma [*Heiken and Wohletz*, 1985]. To investigate this, we compiled the average size of vesicles and phenocrysts from thin section images of gray and tan pumice clasts for the 18 August 1992 Spurr eruption (C. Gardner, unpublished data, 2001). Average vesicle sizes ranged between 13 and 24 μm. Most vesicles were ~20 μm in diameter but a few were as large as 40–120 μm. Mafic phenocryst sizes had an average length of 86 μm and an average width of 52 μm. Plagioclase phenocryst sizes had an average length of 154 μm and an average width of 75 μm.

[49] Vesicle diameters of about 20 μm explain the abundance of nonvesicular particles in smaller size fractions of the Spurr ashes. Particles larger than the vesicle sizes tend to be in the vesicular class and likely have a lower density. Fragmentation for particles with feret averages of 20–80 μm (TV = 3.7–18 cm/s) would be affected by the size of mafic phenocrysts, large vesicles, and small plagioclase phenocrysts, because breakage of these phenocrysts is less likely than simple liberation (breakage along edges). Fragmentation for larger particles >80 μm (TV >18 cm/s) would be primarily influenced by the size of abundant plagioclase phenocrysts. The peak at ~100 μm (TV = 21.5 cm/s) thus reflects the existence of a phenocryst population of approximately that size which tends to be liberated, rather than breaking. So, the peaks in the combined mean curves for Spurr reveal important information regarding fragmentation mechanisms which, in turn, determine the shapes of particles.

[50] Neither the Fuego or Ash Hollow samples had noticable peaks in their shape and size parameter curves. For Fuego, phenocrysts are much larger (>200 μm) and are likely to have been subject to rapid turbulent flow fallout which makes them absent from the distal sample studied. In the case of Ash Hollow, there are no obvious phenocrysts and presumably this reflects either an aphyric magma or large phenocrysts lost by fallout, as in the case of Fuego.

6. Conclusions

[51] To improve our understanding of volcanic ash transport and remote sensing measurements of volcanic clouds, we need quantitative data for fine ash particle shapes (<200 μm diameter). This study developed an accurate methodology for characterizing the shape and size of individual fine ash particles using image analysis. In addition, the terminal velocities of these particles were measured using an air elutriation device called the Roller analyzer. To demonstrate the method on a variety of ashes, we studied distal fallout particles from basalt (Fuego, 1974), andesite (Spurr, 1992), and rhyolite (Ash Hollow, Miocene) eruptions.

[52] The most distinctive shape parameter measured was aspect ratio, which varied greatly from a sphere (1.0) and was 1.5 for the andesitic and basaltic ashes and 1.5–2.6 for the rhyolitic ash. Roughness and sphericity parameters, which use measurements of perimeter and convex perimeter, also provided important shape information. Particle roughness values were similar for all ashes (0.9–1.0 for Spurr and Fuego, and 1.0 for Ash Hollow) and close to 1.0, but even small changes in surface roughness (<10%) could significantly affect terminal velocity. Sphericities (0.6–0.9 for Spurr, 0.6–0.8 for Fuego and Ash Hollow) showed particles differed greatly from a sphere (1.0).

[53] The most useful size parameter is feret diameter since it measures the particle in 64 directions to get an average diameter. The feret diameter measurements for the three ash samples were compared with the diameter of spheres which would fall at the same terminal velocity as that measured for the ashes. The ideal spheres were larger than the ash at fine sizes (feret diameter <25 μm) due to aggregation in the Roller analyzer. Coarser ash was 10–60%, 10–80%, and 40–120% larger (basalt, andesite, and rhyolite, respectively) than ideal spheres.

[54] BET surface areas of fine ashes were as much as one (rarely two) orders of magnitude greater than calculated values for particles using simplified geometric shapes, suggesting that the irregular shapes of ash particles and porosities contribute greatly to surface area. Correction factors (F) for three ash compositions, which relate calculated surface areas to real surface areas, were derived (F = 14 for Fuego, F = 7 for Spurr, and F = 38 for Ash Hollow) and provide a useful way for researchers using similar ash compositions to estimate surface area. Measured perimeters were found to be 1.5 (Spurr and Fuego) to 2 (Ash Hollow) times greater than calculated spherical equivalent perimeters.

[55] One of the ash samples studied (Spurr) showed that phenocrysts and vesicles influenced fragmentation and were important determinants of the resulting shape and size of

particles. Thus size distribution data for ashes should be accompanied by information about vesicles, phenocrysts, and microphenocrysts.

References

Allen, J. R. L., *Sedimentary Structures: Their Character and Physical Basis*, vol. 1, pp. 183–188, Elsevier Sci., New York, 1984.

Armienti, P., G. Macedonio, and M. T. Pareschi, A numerical model for simulation of tephra transport and deposition: Applications to May 18, 1980, Mount St. Helens eruption, *J. Geophys. Res.*, 93, 6463–6476, 1988.

Bluth, G. J. S., C. J. Scott, I. E. Sprod, C. C. Schnetzler, A. J. Krueger, and L. S. Walter, Explosive SO$_2$ emissions from the 1992 eruptions of Mount Spurr, Alaska, *U.S. Geol. Surv. Bull.*, 2139, 37–45, 1995.

Bonadonna, C., G. G. J. Ernst, and R. S. J. Sparks, Thickness variations and volume estimates of tephra fall deposits: The importance of particle Reynolds number, *J. Volcanol. Geotherm. Res.*, 81, 173–187, 1998.

Brazier, S., A. N. Davis, H. Sigurdsson, and R. S. J. Sparks, Fallout and deposition of volcanic ash during the 1979 explosive eruption of the Soufriere of St. Vincent, *J. Volcanol. Geotherm. Res.*, 14, 335–359, 1982.

Brunauer, S., *Physical Adsorption*, Princeton Univ. Press, Princeton, N. J., 1945.

Bursik, M. I., et al., Tephra dispersal, in *The Physics of Explosive Eruptions*, edited by J. S. Gilbert and R. S. J. Sparks, *Geol. Soc. Spec. Publ.*, 145, 115–144, 1998.

Carey, S., and H. Sigurdsson, Influence of particle aggregation on deposition of distal tephra from the May 18, 1980, eruption of Mount St. Helens Volcano, *J. Geophys. Res.*, 87, 7061–7072, 1982.

Casadevall, T. J., and M. D. Krohn, Effects of the 1992 Crater Peak eruptions on airports and aviation operations in the United States and Canada, *U.S. Geol. Surv. Bull.*, 2139, 205–220, 1995.

Center for Nuclear Waste Regulatory Analyses, Ashplume version 1. 0—A code for contaminated ash dispersal and deposition, Southwest Res. Inst., San Antonio, Tex., 1997.

Corey, A. T., Influence of shape on the fall velocity of sand grains, M.S. thesis, Colo. State Univ., Fort Collins, 1949.

Eichelberger, J. C., T. E. C. Keith, T. P. Miller, and C. S. Nye, The 1992 eruptions of Crater Peak Vent, Mount Spurr, Alaska: Chronology and summary, *U.S. Geol. Surv. Bull.*, 2139, 1–18, 1995.

Ernst, G. G. J., M. I. Bursik, S. N. Carey, and R. R. J. Sparks, Sedimentation from turbulent jets and plumes, *J. Geophys. Res.*, 101, 5575–5589, 1996.

Fisher, R. V., Settling velocity of glass shards, *Deep Sea Res.*, 12, 345–353, 1964.

Frye, J. C., A. B. Leonard, and A. Swineford, Stratigraphy of the Ogallala Formation (Neogene) of northern Kansas, *State Geol. Surv. Kansas Bull.*, 118, 90 pp., 1995.

Gardner, C. A., K. V. Cashman, and C. A. Neal, Tephra-fall deposits from the 1992 eruption of Crater Peak, Alaska: Implications of clast textures for eruptive processes, *Bull. Volcanol.*, 59, 537–555, 1998.

Gilbert, J. S., and S. J. Lane, The origin of accretionary lapilli, *Bull. Volcanol.*, 56, 398–411, 1994.

Glaze, L. S., and S. Self, Ashfall dispersal for the 16 September, 1986 eruption of Lascar, Chile, calculated by a turbulent diffusion model, *Geophys. Res. Lett.*, 18, 1237–1240, 1991.

Heiken, G., and K. Wohletz, *Volcanic Ash*, 246 pp., Univ. of Calif. Press, Berkeley, 1985.

Hildreth, W., and R. E. Drake, Volcan Quizapu, Chilean Andes, *Bull. Volcanol.*, 54, 93–125, 1992.

Hoblitt, R. P., and R. S. Harmon, Bimodal density distribution of crypto-dome dacite from the 1980 eruption of Mount St. Helens, Washington, *Bull. Volcanol.*, 55, 421–437, 1993.

Holasek, R. E., A. W. Woods, and S. Self, Experiments on gas-ash separation processes in volcanic umbrella clouds, *J. Volcanol. Geotherm. Res.*, 70, 169–181, 1996.

Jarzemba, M. S., P. A. LaPlante, and K. J. Poor, Ashplume version 1. 0—A code for contaminated ash dispersal and deposition: Technical description and user's guide, Cent. for Nucl. Waste Regul. Anal., Southwest Res. Inst., San Antonio, Tex., 1997.

Jayaweera, K. O. L. F., and B. J. Mason, The behaviour of freely falling cylinders and cones in a viscous fluid, *J. Fluid Mech.*, 22, 709–720, 1965.

Komar, P. D., and C. E. Reimers, Grain shape effects on settling rates, *J. Geol.*, 86, 193–209, 1978.

Krotkov, N. A., A. J. Krueger, and P. K. Bhartia, Ultraviolet optical model of volcanic clouds for remote sensing of ash and sulfur dioxide, *J. Geophys. Res.*, 102, 21,891–21,904, 1997.

Krotkov, N. A., D. E. Flittner, A. J. Krueger, A. Kostinski, C. Riley, W. I. Rose, and O. Torres, Effect of particle non-sphericity on satellite monitoring of drifting volcanic ash clouds, *J. Quant. Spectrosc. Radiat. Transfer*, 63, 613–630, 1999a.

Krotkov, N. A., O. Torres, C. Seftor, A. J. Kruegar, A. Kostinski, W. I. Rose, G. J. S. Bluth, D. Schneider, and S. J. Schaefer, Comparison of TOMS and AVHRR volcanic ash retrievals from the August 1992 eruption of Mt. Spurr, *Geophys. Res. Lett.*, 26, 455–458, 1999b.

Lane, S. J., and J. S. Gilbert, Electric potential gradient changes during explosive activity at Sakurajima volcano, Japan, *Bull. Volcanol.*, 54, 590–594, 1992.

McGimsey, R. G., C. A. Neal, and C. M. Riley, Areal distribution, thickness, mass, volume, and grain size of tephra-fall deposits from the 1992 eruptions of Crater Peak vent, Mt. Spurr volcano, Alaska, *U.S. Geol. Surv. Open File Rep.*, 01–370, 2001.

McNown, J. S., and J. Malaika, Effects of particle shape on settling velocity at low Reynolds number, *Eos Trans. AGU*, 31(1), 74–82, 1950.

Mishchenko, M. I., Light scattering by size-shape distributions of randomly oriented axially symmetric particles of a size comparable to a wavelength, *Appl. Opt.*, 32, 4652–4666, 1993.

Murrow, P. J., W. I. Rose, and S. Self, Determination of the total grain size distribution in a vulcanian eruption column, and its implications to stratospheric aerosol perturbation, *Geophys. Res. Lett.*, 7, 893–896, 1980.

Neal, C. A., R. G. McGimsey, C. A. Gardner, M. L. Harbin, and C. J. Nye, Tephra-fall deposits from the 1992 eruption of Crater Peak, Mount Spurr, Volcano, Alaska: A preliminary report on distribution, stratigraphy, and composition, *U.S. Geol. Surv. Bull.*, 2139, 65–79, 1995.

Perkins, M. E., W. P. Nash, F. H. Brown, and R. J. Fleck, Fallout tuffs of Trapper Creek Idaho—A record of Miocene explosive volcanism in the Snake River Plains volcanic province:, *Geol. Soc. Am. Bull.*, 107, 1484–1506, 1995.

Pettyjohn, E. S., and E. B. Christiansen, Effect of particle shape on free-settling rates of isometric particles, *Chem. Eng. Prog.*, 44(2), 157–172, 1948.

Roller, P. S., Accurate air separator for fine powders, *Ind. Eng. Chem.*, 3(2), 213–216, 1931a.

Roller, P. S., Measurement of particle size with an accurate air analyzer: The fineness and particle size distribution of Portland cement, *U.S. Bur. Mines Tech. Pap.*, 400, 607–628, 1931b.

Rose, W. I., Scavenging of volcanic aerosol by ash: Atmospheric and volcanologic implications, *Geology*, 5, 621–624, 1977.

Rose, W. I., A. T. Andersen, L. G. Woodruff, and S. B. Bonis, The October 1974 basaltic tephra from Fuego Volcano: Description and history of the magma body, *J. Volcanol. Geotherm. Res.*, 4, 3–53, 1978.

Rose, W. I., G. J. S. Bluth, D. J. Schneider, G. G. J. Ernst, C. M. Riley, L. J. Henderson, and R. J. McGimsey, Observations of volcanic clouds in their first few days of atmospheric residence: The 1992 eruptions of Crater Peak, Mount Spurr Volcano, Alaska, *J. Geol.*, 109, 677–694, 1992.

Rose, W. I., A. B. Kostinski, and L. Kelley, Real time C band Radar observations of 1992 eruption clouds from Crater Peak, Mount Spurr Volcano, Alaska, *U.S. Geol. Surv. Bull.*, 2139, 19–28, 1995.

Sarna-Wojcicki, A. M., S. Shipley, R. B. Waitt, D. Dzurisin, and S. H. Wood, Areal distribution, thickness, mass, volume, and grain size of airfall ash from the six major eruptions of 1980, *U.S. Geol. Surv. Prof. Pap.*, 1250, 577–600, 1981.

Schneider, D. J., W. I. Rose, and C. Kelley, Tracking of 1992 Eruption Clouds from Crater Peak Vent of Mount Spurr Volcano, Alaska, using AVHR, *U.S. Geol. Surv. Bull.*, 2139, 27–36, 1995.

Schneider, D. J., W. I. Rose, L. R. Coke, G. J. S. Bluth, I. E. Sprod, and A. J. Krueger, Early evolution of a stratospheric volcanic eruption cloud as observed with TOMS and AVHRR, *J. Geophys. Res.*, 104, 4037–4050, 1999.

Sparks, R. S. J., M. I. Bursik, G. J. Ablay, R. M. E. Thomas, and S. N. Carey, Sedimentation of tephra by volcanic plumes. Part 2: Controls on

thickness and grain-size variations of tephra fall deposits, *Bull. Volcanol.*, *54*, 685–695, 1992.

Sparks, R. S. J., M. I. Bursik, S. N. Carey, J. S. Gilbert, L. S. Glaze, H. Sigurdsson, and A. W. Woods, *Volcanic Plumes*, 574 pp., John Wiley, Hoboken, N. J., 1997.

Stringham, G. E., D. B. Simons, and H. P. Guy, The behavior of large particles falling in quiescent liquids, *U.S. Geol. Surv. Prof. Pap., 562–C*, 36 pp., 1969.

Suzuki, T., A theoretical model for dispersion of tephra, in *Arc Volcanism: Physics and Tectonics*, edited by D. Shimozuru and I. Yokoyama, pp. 95–113, Terra Sci., Tokyo, 1983.

Swinehart, J. B., V. L. Souders, H. M. DeGraw, and R. F. Diffendal Jr., Cenozoic paleogeography of western Nebraska, in *Cenozoic Paleogeography of West-Central United States, Proc. Rocky Mt. Paleogeogr. Symp. 3*, edited by R. M. Flores and S. S. Kaplan, pp. 209–229, Soc. of Econ. Paleontol. and Mineral., Denver, Colo., 1985.

Wadell, H., Sphericity and roundness of rock particles, *J. Geol.*, *86*, 443–451, 1932.

Walker, G. P. L., L. Wilson, and E. L. G. Bowell, Explosive volcanic eruptions–I: The rate of fall of pyroclasts, *Geophys. J. R. Astron. Soc.*, *22*, 377–383, 1971.

Wen, S., and W. I. Rose, Retrieval of sizes and total masses of particles in volcanic clouds using AVHRR bands 4 and 5, *J. Geophys. Res.*, *99*, 5421–5431, 1994.

Williams, H., F. J. Turner, and C. M. Gilbert, *Petrography: An Introduction to the Study of Rocks in Sections*, 72 pp., W. H. Freeman, New York, 1954.

Wilson, L., and T. C. Huang, The influence of shape on the atmospheric settling velocity of volcanic ash particles, *Earth Planet. Sci. Lett.*, *44*, 311–324, 1979.

Zingg, T., Beitrage zur Schotteranalyse, *Schweiz. Mineral. Petrograph. Mitt.*, *15*, 39 pp., 1935.

————————————

G. J. S. Bluth and W. I. Rose, Department of Geological Engineering and Sciences, Michigan Technological University, 1400 Townsend Drive, Houghton, MI 49931, USA.

C. M. Riley, School of Education and Social Policy, Northwestern University, Evanston, IL 60201, USA. (c-riley@northwestern.edu)